

Supplementary Information

Augmenting immunotherapy via bioinspired MOF-based ROS homeostasis disruptor with nanozyme-cascade reaction

Ruifang Wang^{a,b+}, Maosong Qiu^{a,b+}, Lei Zhang^{a,b,c+}, Meiju Sui^{a,b}, Long Xiao^{a,b}, Qiao Yu^{a,b}, Chaohui Ye^{a,b,c}, Shizhen Chen^{a,b,c*}, Xin Zhou^{a,b,c*}

^a Key Laboratory of Magnetic Resonance in Biological Systems, State Key Laboratory of Magnetic Resonance and Atomic and Molecular Physics, National Center for Magnetic Resonance in Wuhan, Wuhan Institute of Physics and Mathematics, Innovation Academy for Precision Measurement Science and Technology, Chinese Academy of Sciences-Wuhan National Laboratory for Optoelectronics, Huazhong University of Science and Technology, Wuhan 430071, P. R. China.

^b University of Chinese Academy of Sciences, Beijing 100049, P. R. China.

^c Optics Valley Laboratory, Hubei 430074, P.R. China.

* Corresponding author: xinzhou@wipm.ac.cn; chenshizhen@wipm.ac.cn.

⁺ These authors contributed equally to this work

Table of Contents

Materials	S-3
Characterization of the CMZM.....	S-4
SDS-PAGE and Coomassie bright blue staining	S-4
The SOD-like activity of CMZM.....	S-5
·OH production by the POD-like activity of CMZM.....	S-5
O ₂ generation ability by the CAT-like activity of CMZM	S-5
¹ O ₂ generation ability of CMZM	S-6
Electron spin resonance (ESR) assay	S-6
GSH eliminated ability by the GSHOx-like activity of CMZM.....	S-7
<i>In vitro</i> ¹ H/ ¹⁹ F MRI	S-7
Cell culture.....	S-8
Cytotoxicity of CMZM.....	S-8
Cell uptake of CMZM	S-8
<i>In vitro</i> homologous targeting assay	S-9
<i>In vitro</i> immune escape assay	S-9
Intracellular reactive oxygen species (ROS) detection	S-9
<i>In vitro</i> CDT&PDT therapeutic efficiency	S-10
Animal and tumor models	S-10
<i>In vivo</i> fluorescence imaging	S-11
Hemolysis assay	S-11

Materials

Except where otherwise noted, all chemicals were used without further purification. Zn(OAc)₂·2H₂O, manganese acetylacetonate, 2-methylimidazole (2-MIM), 4-(trifluoromethyl)-¹H-imidazole (TFMIM), methanol, chlorin e6 (Ce6), methylene blue (MB), and ammonia solution (NH₃·H₂O) were acquired from Macklin (Shanghai, China). Methanol and H₂O₂ were received from Shanghai Hushi Chemical Co., Ltd. Cu/Zn-SOD and Mn-SOD Assay Kit with WST-8 were obtained from Beyotime Biotechnology (S0103). Methylene blue (MB) was purchased from Adamas-beta (Shanghai, China). 5,5'-Dithiobis (2-nitrobenzoic acid) (DTNB), 1,3-Diphenylisobenzofuran (DPBF) were obtained from Bide Pharmatech Ltd (Shanghai, China). 5,5-dimethyl-1-pyrroline N-oxide (DMPO) and 2,2,6,6-Tetramethyl-4-piperidone hydrochloride (TEMP) was obtained from Sigma-Aldrich (Shanghai, China). 2',7'-dichlorodihydrofluorescein diacetate (DCFH-DA) and 4',6-diamidino-2-phenylindole (DAPI) were purchased from Solarbio (Beijing, China). Calcein/PI cell viability/cytotoxicity Assay Kit and Annexin V-FITC /PI Apoptosis Kit were obtained from Beyotime Biotechnology (Shanghai, China). Antibodies against CD45, CD3, CD4, CD8, CD25, FOXP3, CD11b, F4/80, CD80, CD86, CD206, CD11c, and MHCII for flow cytometry were purchased from Thermo Fisher (Waltham, USA). PE anti-mouse CD274 (B7-H1) was purchased from BioLegend (USA). Mouse TNF-α ELISA Kit, Mouse IL-6 ELISA Kit, Mouse IL-10 ELISA Kit, Mouse IL-12 ELISA Kit, and Mouse IL-16 ELISA Kit were obtained from Solarbio (China).

Characterization of the CMZM

The morphology structures of CMZ and CMZM were observed by the TEM (FEI Company, USA). The elements distribution of CMZ was displayed by the HAADF-STEM (Oxford x-met 8000). Dynamic light scattering (DLS) and zeta potential measurements were conducted by a ZS nanohybrid analyzer (Malvern, England). Ultraviolet-visible-near infrared (UV-vis-NIR) absorption spectra of different samples were recorded by an Evolution 220 UV-vis spectrophotometer (Thermo Fisher Scientific Inc., USA). The values of Mn in different valence states were analyzed using XPS (ESCA Lab 250, Thermo Fisher Scientific, USA) experiments. The Mn concentration of the samples was measured by ICP-OES (Agilent 5110, USA) or ICP-MS (PQ-MS, Germany). The surface area and pore diameter distribution were obtained on the nitrogen adsorption apparatus (ASAP 2420, Micromeritics, USA). The crystalline structures were evaluated by X-ray diffraction (XRD) analysis on a D8 Focus diffractometer (Bruker, Germany). All *in vitro* and *in vivo* ^1H MRI and ^{19}F MRI experiments were performed on a 9.4 T micro-imaging system (Bruker Avance 400, Ettlingen, Germany).

SDS-PAGE and Coomassie bright blue staining

The protein expression profiles of CMZ, CMZM, and 4T1 cell membrane were measured by SDS-PAGE and Coomassie bright blue staining. In brief, the different samples plus the SDS-PAGE gel loading buffer was heated in a boiling water bath for twenty min. And the proteins were separated through 12% polyacrylamide gel by the

Mini-PROTEAN Tetra System (BIO-RAD, CA, USA). Finally, the protein gel was stained with the Coomassie brilliant blue and imaged.

The SOD-like activity of CMZM

The SOD-like activity was measured by Cu/Zn-SOD and Mn-SOD Assay Kit with WST-8. In brief, the WST-8 can generate colorful formazan with a robust UV-vis absorbance at 450 nm after reacting with $O_2^{\bullet-}$ produced by xanthine oxidase. Once mixed with nanomaterials with SOD-like enzyme activity, the $O_2^{\bullet-}$ can be converted to water and O_2 , leading to the inhibition of the production of formazan. Specifically, various concentration of CMZM was mixed with WST and xanthine oxidase for 30 min at 37°C. After that, the UV-vis absorbance at 450 nm was monitored. Calculation of percentage inhibition was performed using the following formula: inhibition (%) = $[(A_0 - A_i) / A_0] \times 100\%$, where A_0 and A_i are the absorbances of the control and sample, respectively.

·OH production by the POD-like activity of CMZM

Typically, MB ($5 \mu\text{g mL}^{-1}$), H_2O_2 (10 mM), and CMZM ($200 \mu\text{g mL}^{-1}$) were mixed in $NaHCO_3$ (25 mM) solution and stood at 37°C for 30 min. The ·OH-induced MB degradation was measured by observing the change in absorbance at 665 nm. Besides, the UV-vis-NIR and ^{19}F NMR were used to monitor the concentration-dependent POD-like activity of CMZM.

O_2 generation ability by the CAT-like activity of CMZM

The CAT-like activity of CMZM was monitored at 37°C by measuring the generated oxygen using a dissolved oxygen meter. Specifically, a 50 μL of H_2O_2 (2 M) was added to 2 mL of CMZM (50 $\mu\text{g mL}^{-1}$). The generated O_2 solubility (mg L^{-1}) was measured after different reaction times.

$^1\text{O}_2$ generation ability of CMZM

Singlet oxygen ($^1\text{O}_2$) production was assessed in a solution of CMZM using the 1,3-Diphenylisobenzofuran (DPBF) as a $^1\text{O}_2$ detection probe. Specifically, CMZM (50 $\mu\text{g mL}^{-1}$) with or without H_2O_2 (1 mM) were dispersed in 3 mL of DMF solution containing DPBF (1 mM), and then the mixture was irradiated by a 660 nm laser with a power density of 0.1 W cm^{-2} for different times. Finally, the production of $^1\text{O}_2$ was monitored by a UV-vis spectrophotometer.

Electron spin resonance (ESR) assay

Electron spin resonance (ESR) measurement using the ESR spin trapping technique was used to identify intermediates associated with short-lived free radicals. DMPO and TEMP were used as the trapping agents to monitor the $\cdot\text{OH}$ and $^1\text{O}_2$, respectively. For $\cdot\text{OH}$ detection, CMZM (50 $\mu\text{g mL}^{-1}$) was mixed with H_2O_2 (1.0 mM) and DMPO in NaHCO_3 (25 mM) solution. After mixing evenly, the mixture was transferred to a quartz tube for ESR assay. For the $^1\text{O}_2$ detection, the CMZM (50 $\mu\text{g mL}^{-1}$) in PBS was irradiated with a laser (660 nm, 0.1 W cm^{-2}) for 5 minutes. Then, the solution was mixed with TEMP quickly for ESR assay.

GSH eliminated ability by the GSHOx-like activity of CMZM

Ellman's assay was used to evaluate the GSH-eliminating of CMZM. Specifically, various concentrations of CMZM were mixed with GSH (1 mM) in a 1.5 mL centrifuge tube. After the reaction for 1 h, 200 μ L of DTNB (1 mg mL⁻¹) was added to the mixture. After 10 min, the CMZM was removed by centrifuging at 10000 rpm for 10 min. Finally, the UV-vis absorbance of the supernatant at 410 nm was determined with a UV-vis spectrophotometer. In addition, the GSHOx-like activity of CMZM with different concentrations was determined by the ¹⁹F NMR. All the experiments were performed in the dark and triplicate.

***In vitro* ¹H/¹⁹F MRI**

The ¹H T₁-weighed MRI of the solution was performed on the 9.4 T micro-imaging system (Bruker Avance 400, Ettlingen, Germany). Various concentrations of CMZM based on Mn (C_{Mn} = 0, 0.1, 0.2, 0.4, 0.6, 0.8 1.0 mM) were dispersed into PBS (10 mM, pH 7.4, 6.5, or 5.5) and PBS (10 mM, pH 5.5) containing 10 mM GSH, respectively. After 2 h, a ¹H T₁-weighed MRI of different samples was performed with a RARE sequence (TR = 500 ms, TE = 11 ms, FOV = 3 cm \times 3 cm, 1 mm slice thickness, RARE factor = 4, matrix size = 256 \times 256). For the ¹⁹F MRI, various concentrations of CMZM based on TFMIM (C_{TFMIM} = 0, 2.5, 5, 10, 20, and 50 mM) received the same treatment as ¹H MRI. Finally, the ¹⁹F MRI was performed through a RARE sequence (TR = 800 ms, TE = 3 ms, FOV = 3.7 cm \times 3.7 cm, 25.5 mm slice thickness, matrix size = 32 \times 32, 16 averages).

Cell culture

4T1, Hela, 293T, A549, and RAW264.7 cell lines were purchased from the cell bank of the Chinese Academy of Sciences (Shanghai, China) and cultured with the basic medium that contained 10% FBS, 100 U mL⁻¹ penicillin, and 100 U mL⁻¹ streptomycin under humidified air with 5% CO₂ at 37°C. All agents were purchased from Boster Company (China) and filtered with a 0.2 µm sterile filter before incubation with cells.

Cytotoxicity of CMZM

The cytocompatibility of CMZM on 4T1 cells, A549 cells, Hela cells, and 293T cells was evaluated by using the standard CCK8 assay. The different cells were incubated in a 96-well plate (1×10^4 cells per well) and incubated for 24 h. The CMZM stock solution was diluted to 5, 10, 20, 30, 50, and 100 µg mL⁻¹ using the corresponding medium of various cells and added to the 96-well plate wells. After 24 h, the media was carefully removed and washed with PBS, and incubated with CCK-8 solution for another 2 h at 37°C. Finally, the microplate reader was used to measure the absorbance at 450 nm. The cells cultured with medium without CMZM were used as control. All data are presented as mean ± SD, n = 6.

Cell uptake of CMZM

For the cellular uptake, 4T1 cells were treated with CMZM (50 µg mL⁻¹) at 37°C. After 0.5 h, 2 h, 4 h, and 8 h incubation, the cells were washed with PBS (pH = 7.4)

three times to remove the unabsorbed nanohybrid. Finally, the 4T1 cells were imaged by the CLSM imaging system and used to flow cytometry analysis (Beckman Coulter).

***In vitro* homologous targeting assay**

Briefly, different tumor cells including 4T1, Hela, and A549 cells were seeded into 6-well plates at a density of 1×10^5 cells per well and cultured for 24 h. The CMZM ($50 \mu\text{g mL}^{-1}$) was used to culture with cells for 4 h. Afterward, the cells were collected and analyzed by flow cytometry (Beckman Coulter).

***In vitro* immune escape assay**

The macrophage RAW264.7 cells were used to evaluate the immune escape effects of CMZM. The nanohybrid without 4T1 cell membrane modification was set as control. Specifically, RAW264.7 cells were seeded into 6-well plates at a density of 1×10^5 cells for 24 h. Then, the cells were cultured with CMZ or CMZM for 4 h. Afterward, the cells were washed with PBS and fixed with 4% paraformaldehyde for 10 min, and the nucleus was stained with DAPI for 5 min for the CLSM image. Besides, the cells were collected and analyzed by flow cytometry (Beckman Coulter).

Intracellular reactive oxygen species (ROS) detection

In brief, 4T1 cells were seeded into 6-well plates at a density of 1×10^5 cells per well and treated with different samples (PBS, free Ce6, and CMZM) with or without 660 nm laser irradiation (0.1 W cm^{-2} for 10 min). After that, the cultural media were replaced by fresh cultural media. And then, the 2',7'-dichlorofluorescein diacetate

(DCFH-DA) was added to each well and incubated for 60 min at 37°C. Finally, CLSM was used to visualize the ROS generated in the 4T1 cells.

In vitro CDT&PDT therapeutic efficiency

For the CCK8 assay, the 4T1 cells were seeded into 96-well plates at a density of 1×10^4 cells per well and cultured for 24 h (37°C). Then, the 4T1 cells were incubated with different samples (PBS, free Ce6, and CMZM) with or without 660 nm laser irradiation (0.1 W cm^{-2} for 10 min). After that, the cells were washed with PBS and incubated for another 2 h. The cell viability was analyzed by CCK-8 assay.

Confocal fluorescence imaging analysis: In short, 4T1 cells (1×10^5) were seeded into 6-well plates and incubated with different samples (PBS, free Ce6, and CMZM) for 4 h. After washing three times with PBS, the cells were exposed to 660 nm laser irradiation (0.1 W cm^{-2}) for 10 min or not. Then, the cells were stained with Calcein AM/PI to probe living cells (green) and dead cells (red) and imaged by a confocal laser scanning fluorescence microscope (A1R/A1, Nikon, Japan).

Flow cytometry analysis: The death rate of 4T1 cells with different treatments was determined by flow cytometry. Same to the above CLSM experiments, different treatments of 4T1 cells were collected and stained by Annexin V-FITC/PI for 15 min and analyzed by flow cytometry (Beckman Coulter).

Animal and tumor models

Female Balb/c mice (5-6 weeks of age) were purchased from Beijing Vital River

Laboratory Animal Technology Co., Ltd. All experimental protocols in this study were approved by Animal Care and Use Committees at the Innovation Academy for Precision Measurement Science and Technology, the Chinese Academy of Sciences. In this paper, 4T1 tumor-bearing mice were built by subcutaneous injection with 4T1 cells (100 μL , 5×10^6 cells mL^{-1}) on the leg of the mice.

***In vivo* fluorescence imaging**

The 4T1 tumor-bearing mice were randomly classified into three groups (n=3). The mice were given *i.v.* injections of 100 μL free Ce6, CMZ, and CMZM (with Ce6 concentration of 12 μM) for fluorescence imaging using an IVIS Spectrum imaging system (Perkin Elmer) at 0, 2, 4, 8, 12, 24, and 36 h. Afterward, the mice were sacrificed, and the tumor and main organs (heart, liver, spleen, lung, and kidney) were dissected for *ex vivo* imaging (Ex: 640 nm; Em: 720 nm).

Hemolysis assay

The whole blood samples from healthy Balb/c mice were collected and red blood cells (RBCs) were obtained from serum by centrifugation at 2000 rpm for 10 min. The RBCs were further washed several times with 10 mL of sterile PBS until the supernatant became colorless and transparent. Finally, the RBCs were diluted to 20 mL with sterile PBS. Afterward, The CMZM was added to the erythrocyte suspension to a final concentration of 30, 50, 100, 200, 300, 500, 800, and 1000 $\mu\text{g mL}^{-1}$. After 4 h of cultivation at 37°C, observing and recording the hemolysis phenomenon. At the same time, the specific 540 nm spectrophotometric absorptions of hemoglobin were

monitored. The corresponding hemolysis percentage values were calculated using the following formula: Hemolysis (%) = [(sample absorbance - negative control)/(positive control - negative control)] × 100%. RBCs incubated with deionized water and PBS were used as the positive and negative controls, respectively. All the experiments were repeated three times.

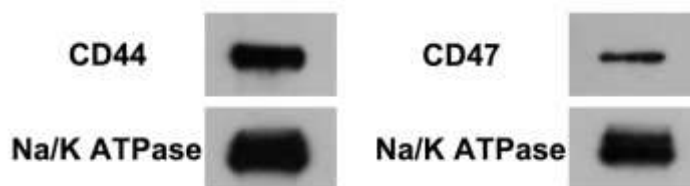


Figure S1. CD44 and CD47 membrane protein characterization by western blotting analysis of CMZM.

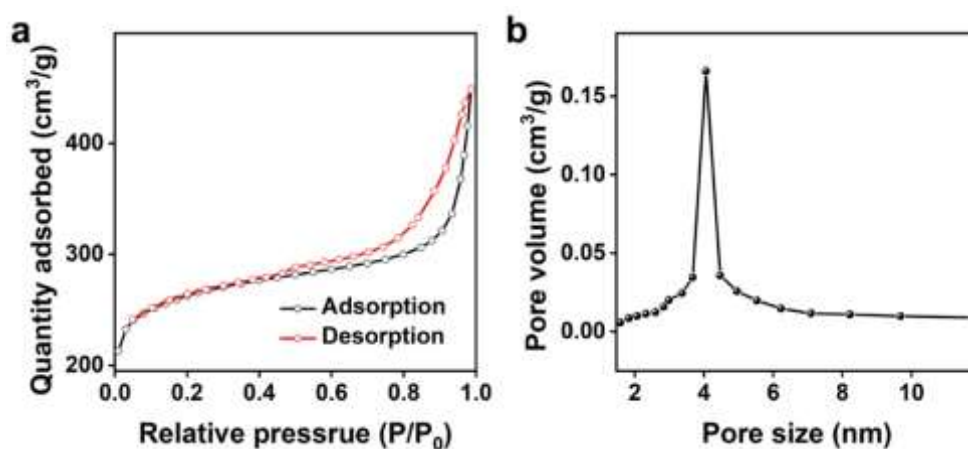


Figure S2. (a) BET analysis and (b) pore size distribution (inset) of Mn-F-ZIF-8.

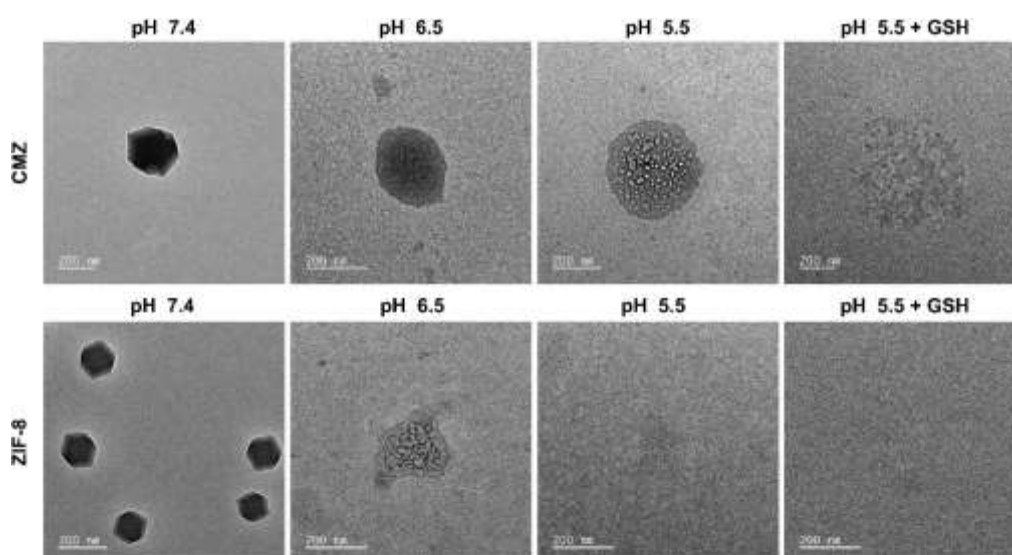


Figure S3. TEM images of CMZ and ZIF-8 after immersion in PB buffer (pH 7.4, pH 6.5, pH 5.5, and pH 5.5 plus GSH (10 mM) for 2 h.

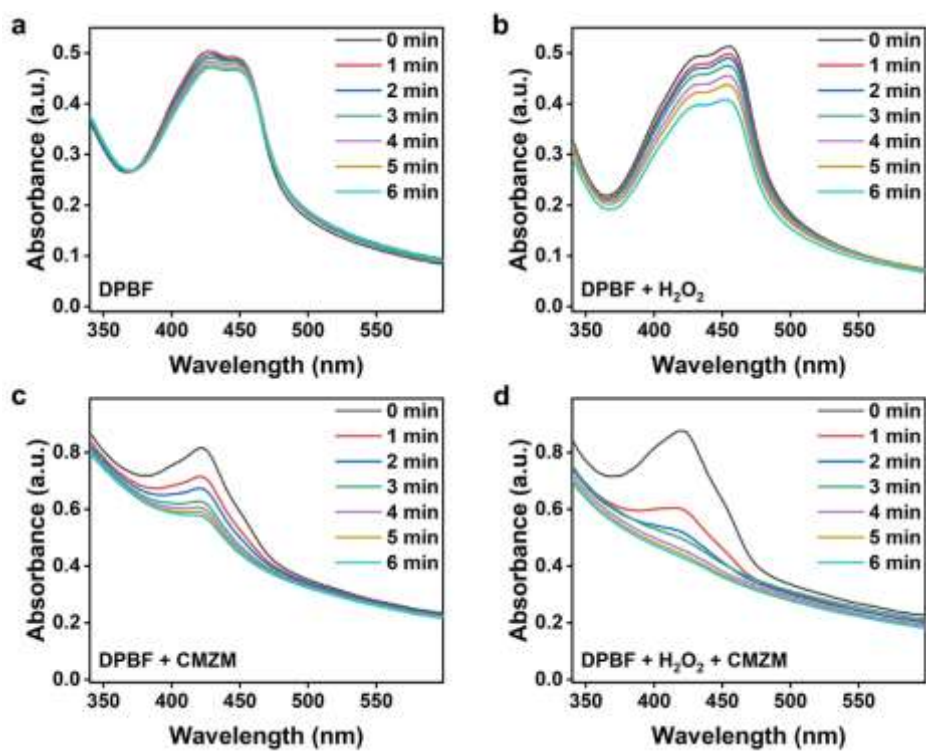


Figure S4. Time-dependent $^1\text{O}_2$ generation (probe by photodegradation of DPBF at 415 nm) of PBS, H_2O_2 , CMZM, and CMZM + H_2O_2 with laser irradiation for 0 to 6 min (660 nm, 0.1 W cm^{-2}).

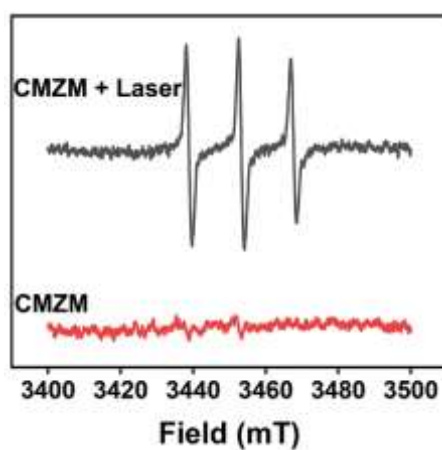


Figure S5. ESR spectra of $^1\text{O}_2$.

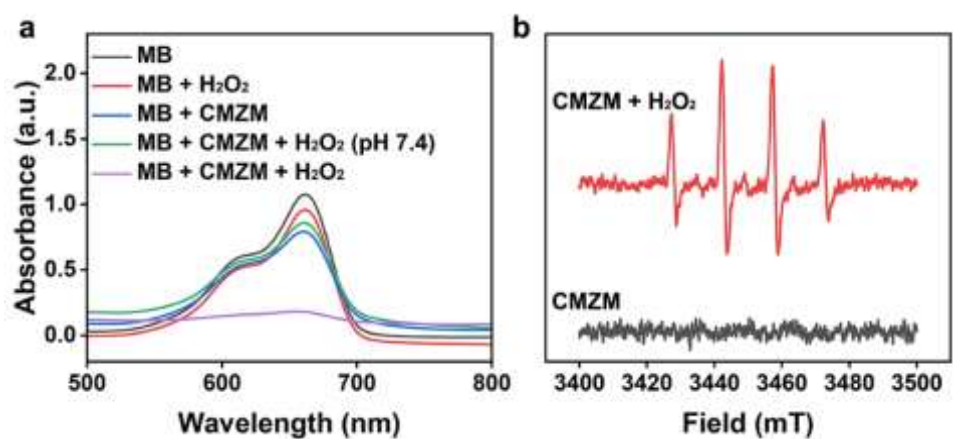


Figure S6. The POD-like activity of CMZM and ESR spectra of •OH.

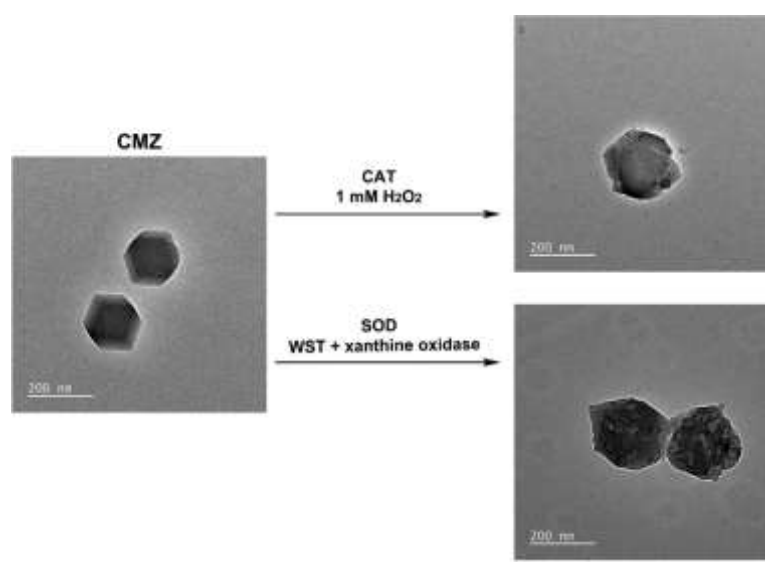


Figure S7. The TEM images of CMZ after treatment with H₂O₂ or WST plus xanthine oxidase.

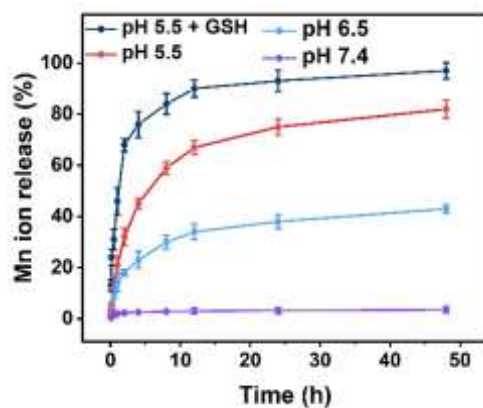


Figure S8. The accumulated release profiles of Mn ion from CMZM in PB buffer (pH 7.4, pH 6.5, pH 5.5, and pH 5.5 plus 10 mM GSH) (mean \pm SD, $n = 3$).

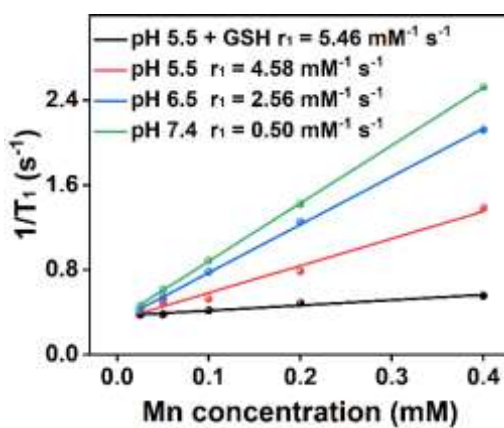


Figure S9. The r_1 value of CMZM with diverse treatments (pH 7.4, pH 6.5, pH 5.5, and pH 5.5 plus 10 mM GSH).

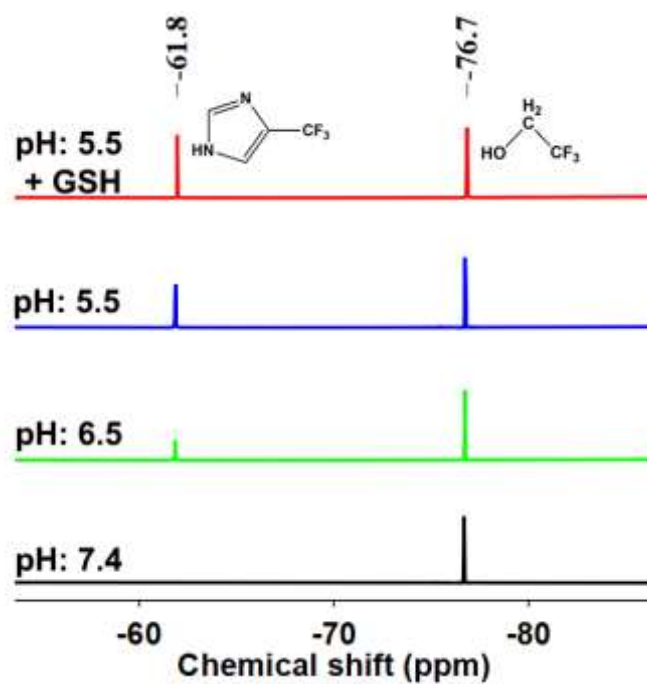


Figure S10. ^{19}F NMR of CMZM in PB buffer (pH 7.4, pH 6.5, pH 5.5, and pH 5.5 plus 10 mM GSH).

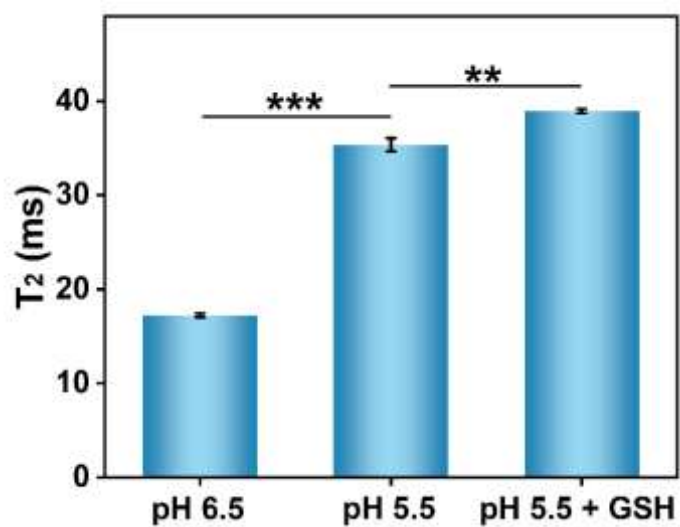


Figure S11. The transverse relaxation times of CMZM (TFMIM: $-\text{CF}_3$) in PB buffer (pH 6.5, pH 5.5, and pH 5.5 plus 10 mM GSH) (mean \pm SD, $n = 3$, $**p < 0.01$, $***p < 0.001$).

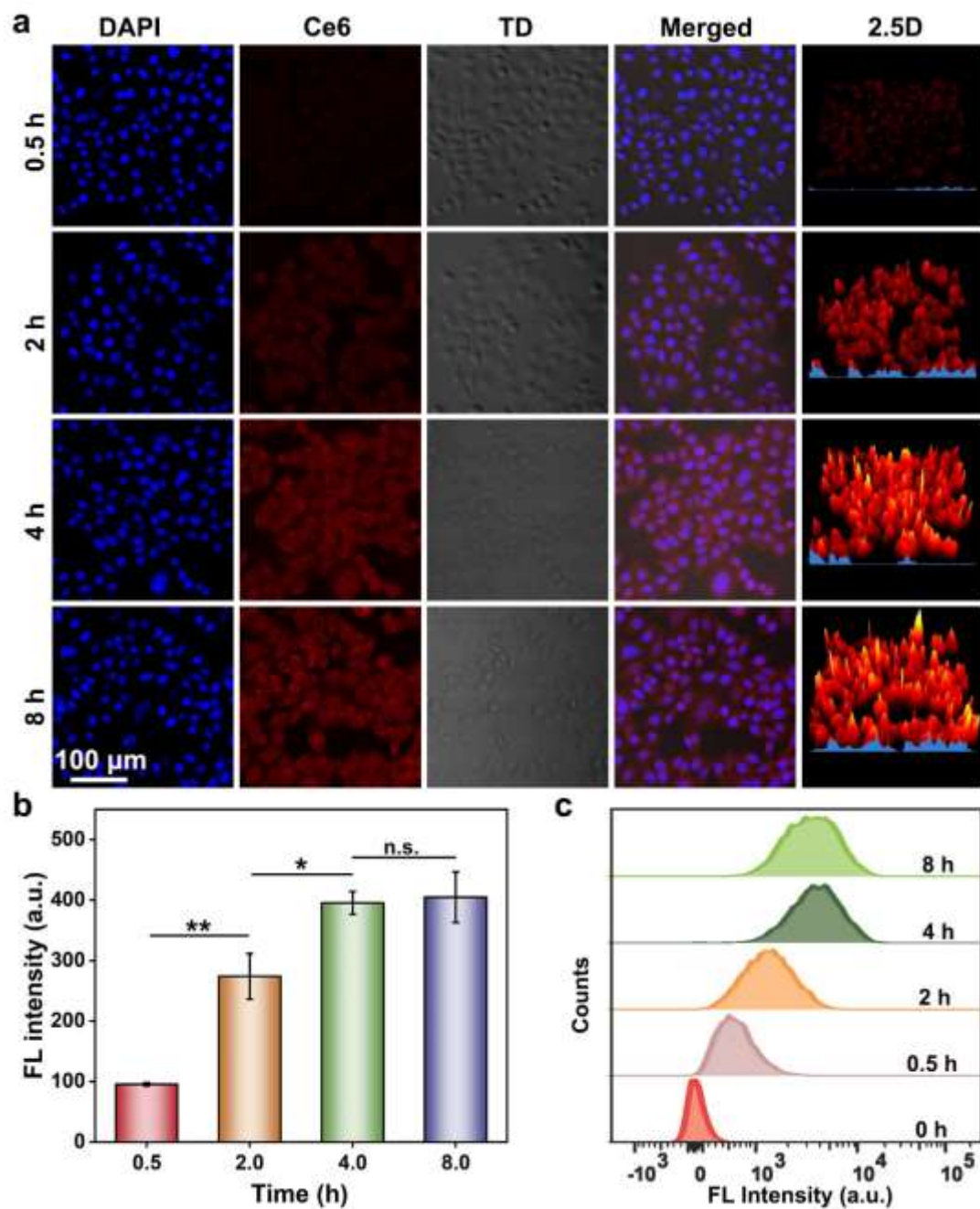


Figure S12. Intracellular uptake of CMZM. (a) CLSM images of 4T1 cells incubated with CMZM for 0.5 h, 2 h, 4 h, and 8 h, respectively, and (b) the corresponding fluorescence intensity analysis of CLSM images (mean \pm SD, $n = 3$, n.s.: no significance, $*p < 0.05$, $**p < 0.01$). (c) Flow cytometry quantification of 4T1 cells incubated with CMZM for different times.

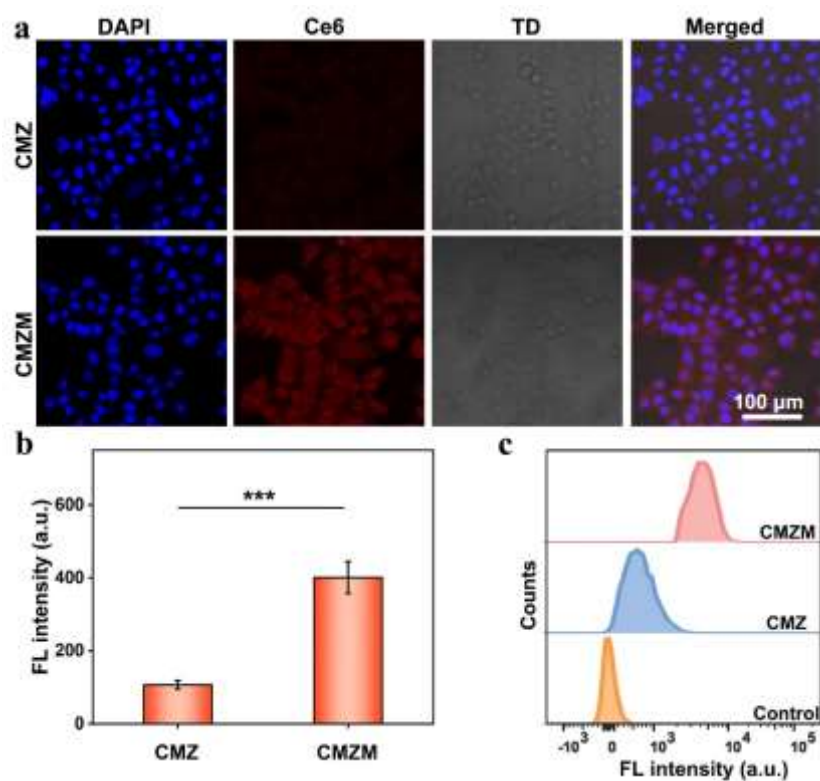


Figure S13. (a) Confocal images of 4T1 cells after being treated with the CMZ and CMZM ($30 \mu\text{g}\cdot\text{mL}^{-1}$) for 4 h. (b) The corresponding fluorescence intensity of Ce6 in 4T1 cells (mean \pm SD, $n = 3$, $***p < 0.01$). (c) Flow cytometry quantification analysis of 4T1 cells incubated with the CMZ and CMZM for 4 h.

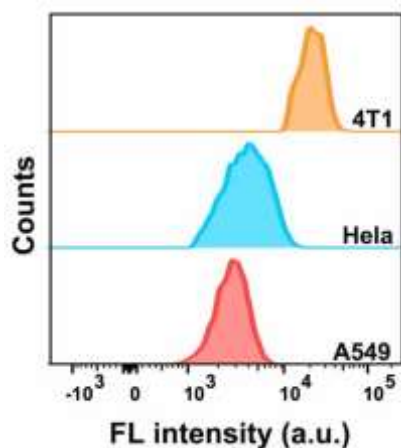


Figure S14. 4T1, HeLa, and A549 cells incubated with CMZM for 4 h were determined by flow cytometry.

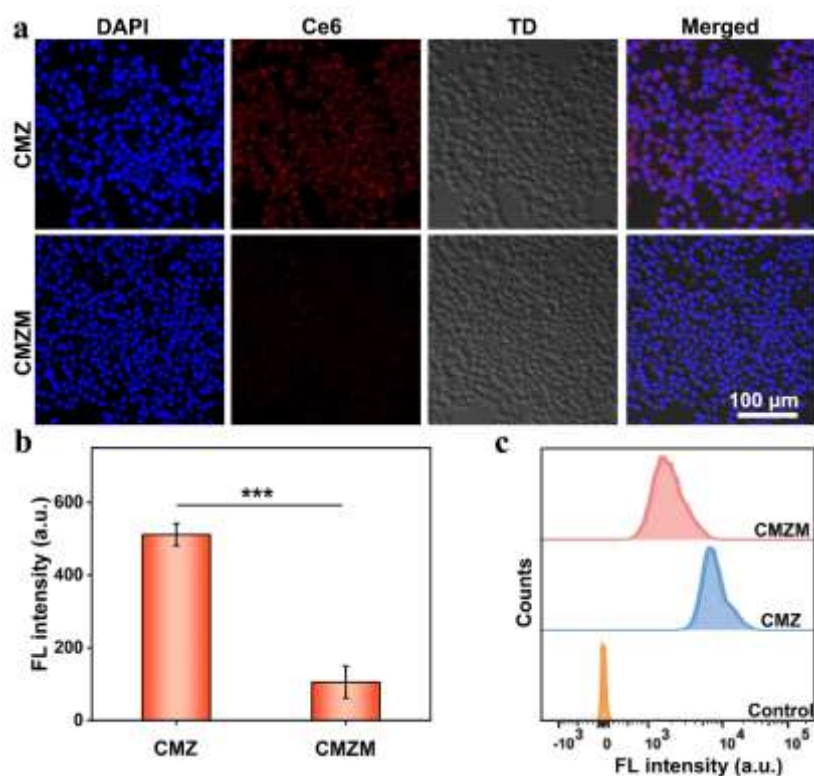


Figure S15. (a) Confocal images of Raw264.7 cells after treatment with CMZ and CMZM ($30 \mu\text{g}\cdot\text{mL}^{-1}$) for 4 h. (b) The corresponding fluorescence intensity of Ce6 in Raw264.7 cells (mean \pm SD, $n = 3$, *** $p < 0.001$). (c) Flow cytometry quantification analysis of Raw264.7 cells incubated with CMZ and CMZM for 4 h.

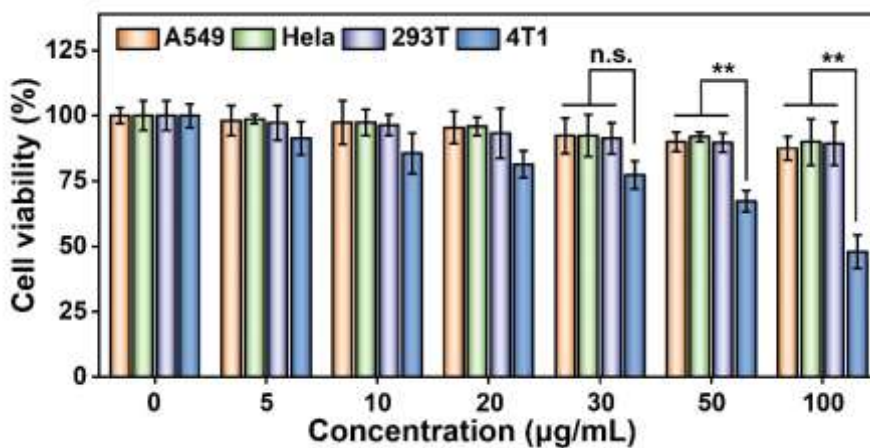


Figure S16. The viability of A549, HeLa, 293T, and 4T1 cells after treatment with CMZM for 24 h (mean \pm SD, $n = 6$, n.s.: no significance, ** $p < 0.01$).

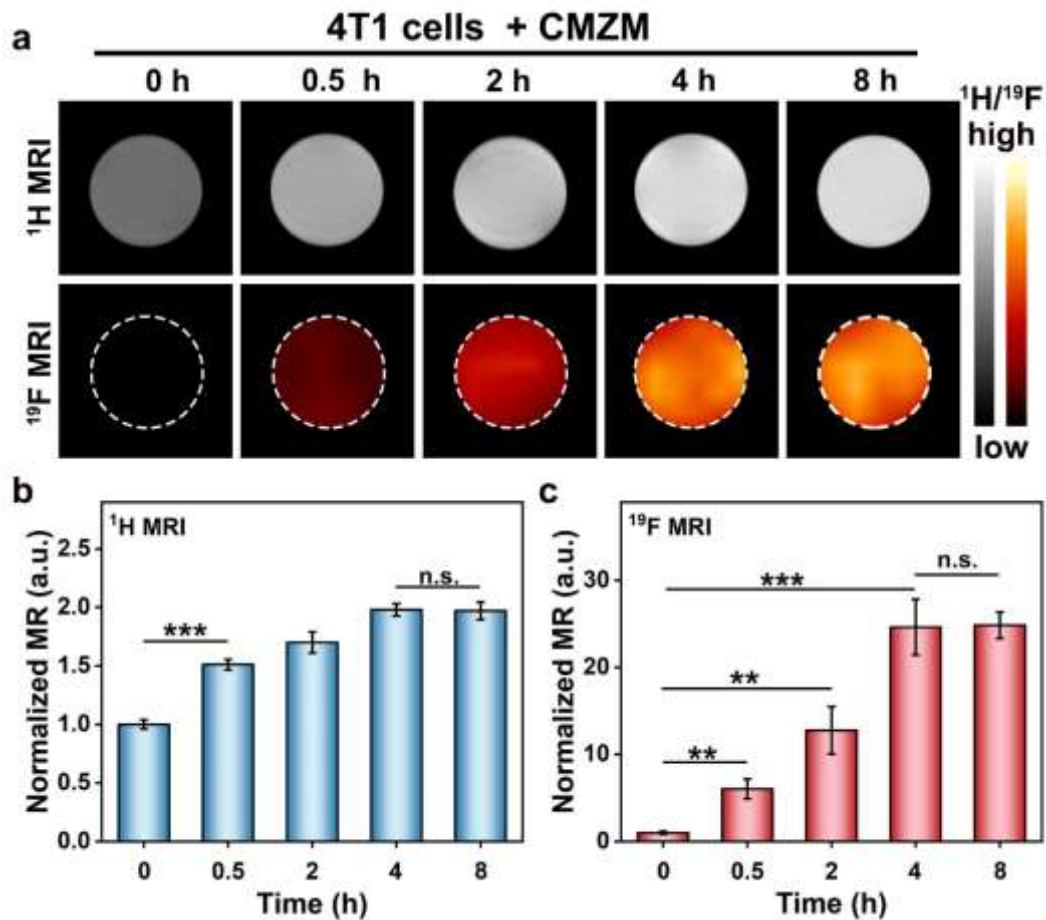


Figure S17. (a) ^1H MRI and ^{19}F MRI of 4T1 cells treated with CMZM at 0, 0.5, 2, 4, and 8 h. The corresponding (b) ^1H MRI and (c) ^{19}F MRI signal intensity of 4T1 cells in (a) (mean \pm SD, $n = 3$, n.s.: no significance, $**p < 0.01$, $***p < 0.001$).

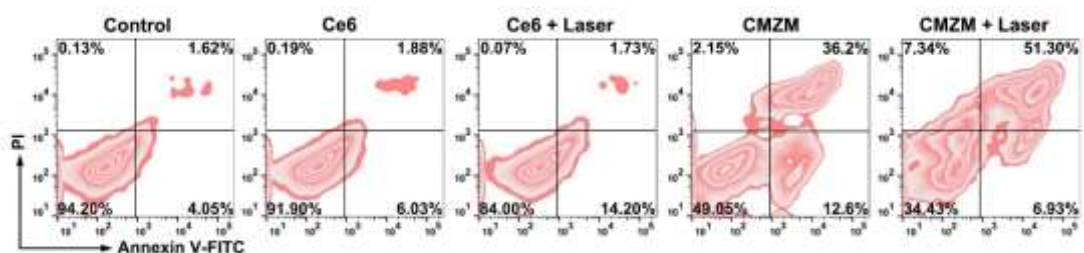


Figure S18. Flow cytometry quantification of 4T1 cell apoptosis after various treatments.

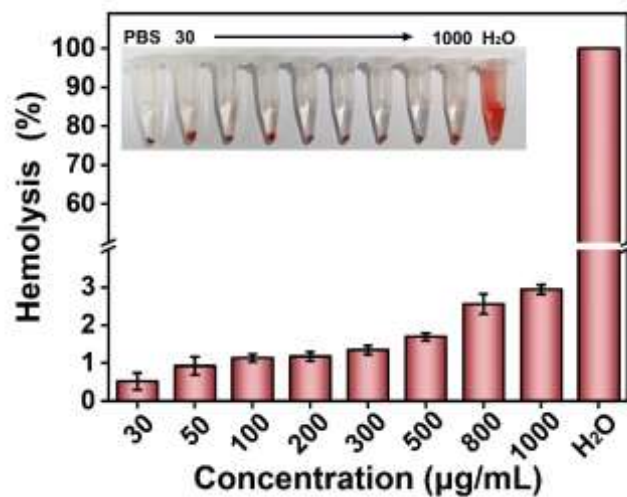


Figure S19. *In vitro* hemolysis percentage of CMZM incubated with mice RBCs at 37°C for 4 h at various concentrations. PBS was set as the negative control and deionized water was set as the positive control. (mean \pm SD, $n = 3$).

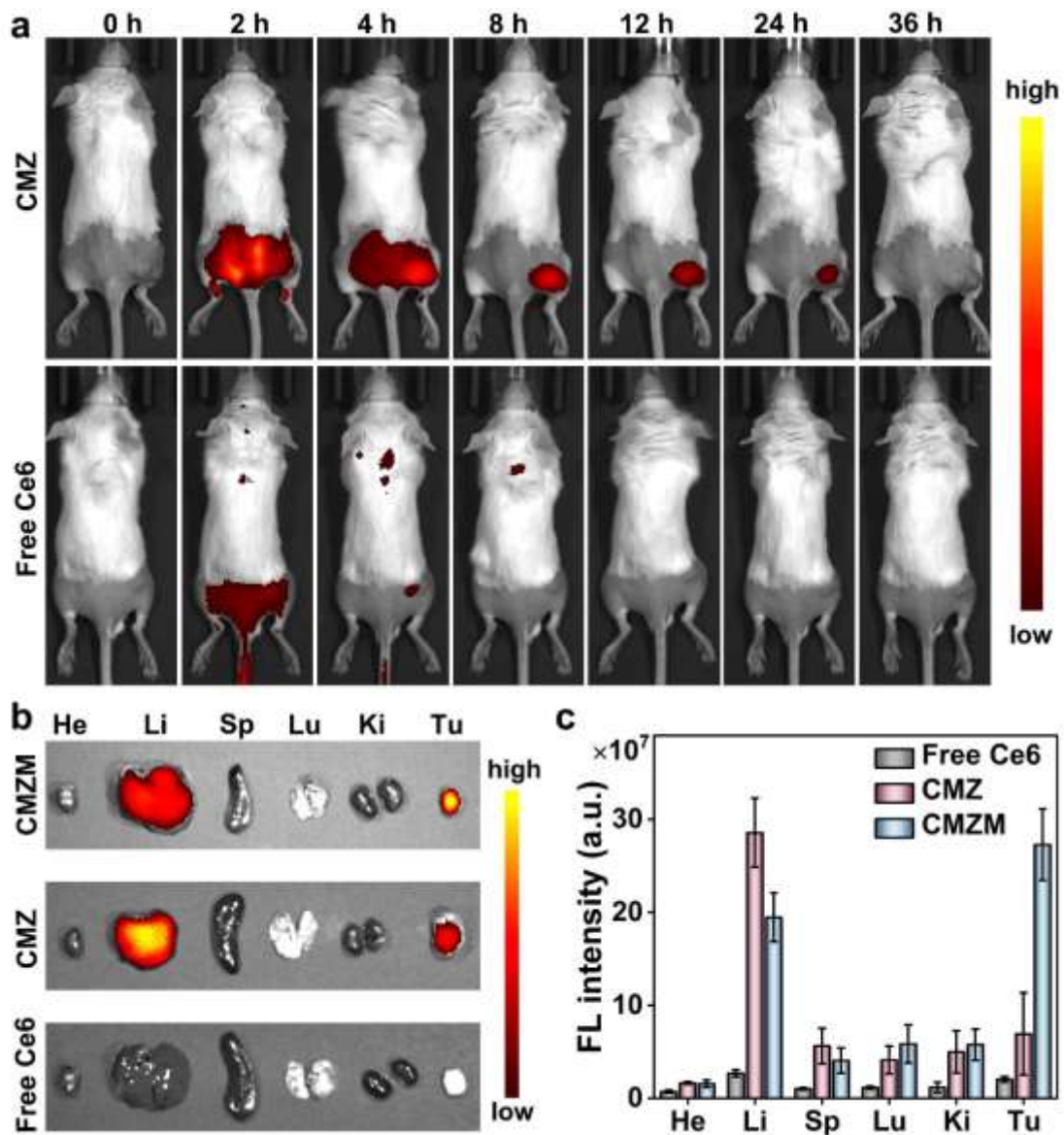


Figure S20. *In vivo* FLI of CMZ and free Ce6. (a) Time-dependent fluorescence imaging of subcutaneous 4T1 tumor-bearing mice after *i.v.* injection of CMZ and free Ce6. (b) Fluorescence imaging and (c) fluorescence intensity quantification of isolated organs in CMZM, CMZ, and free Ce6 groups at 36 h post-injection (mean \pm SD, $n = 3$).

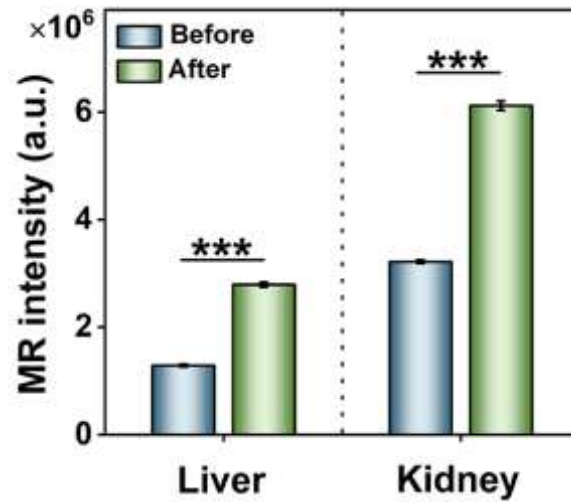


Figure S21. The ¹H MRI signal intensity of the liver and kidney before and 8 h post *i.v.* injection of CMZM (mean ± SD, *n* = 3, ****p* < 0.001).

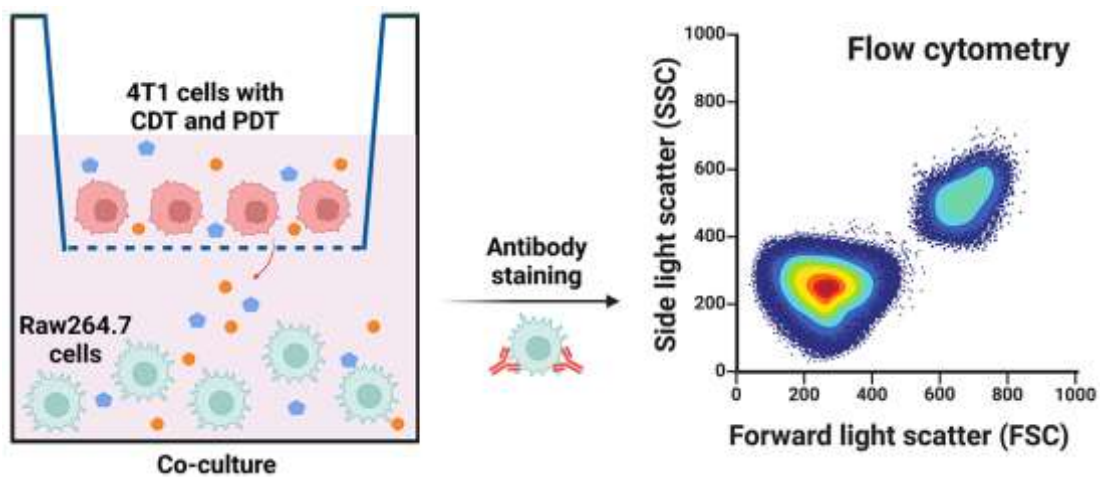


Figure S22. A schematic presentation of M2 macrophages polarized to M1 macrophages via the transwell insert system after various treatments (Control, CMZM, CMZM plus laser).

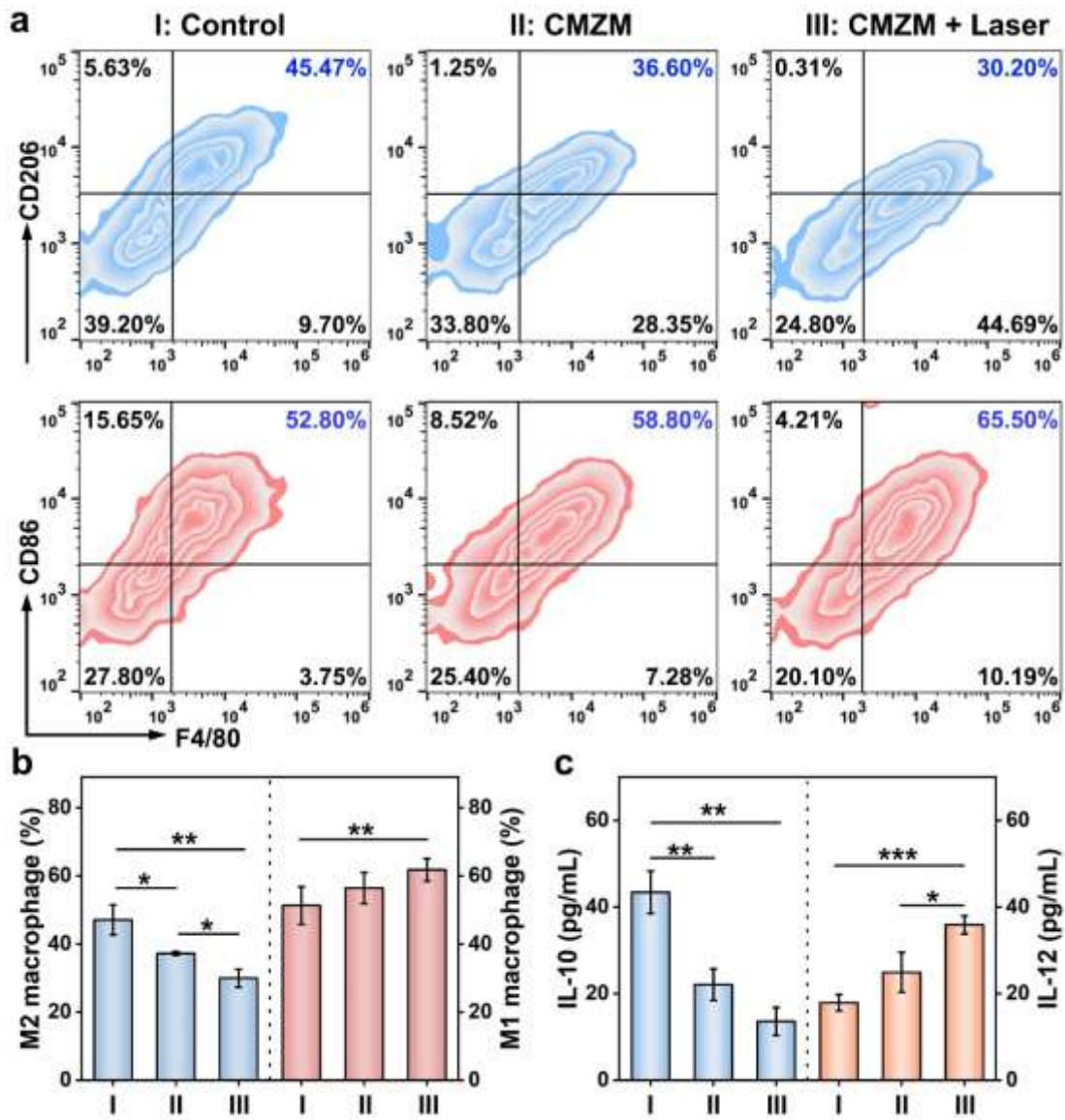


Figure S23. *In vitro* immune activated by CMZM. (a) FCM and (b) the relevant quantitative analysis of M1 phenotype macrophages and M2 phenotype macrophages (mean \pm SD, $n = 3$, $*p < 0.05$ and $**p < 0.01$). (c) The concentration of IL-12 and IL-10 in the supernatant post various treatments (mean \pm SD, $n = 3$, $*p < 0.05$, $**p < 0.01$, $***p < 0.001$).

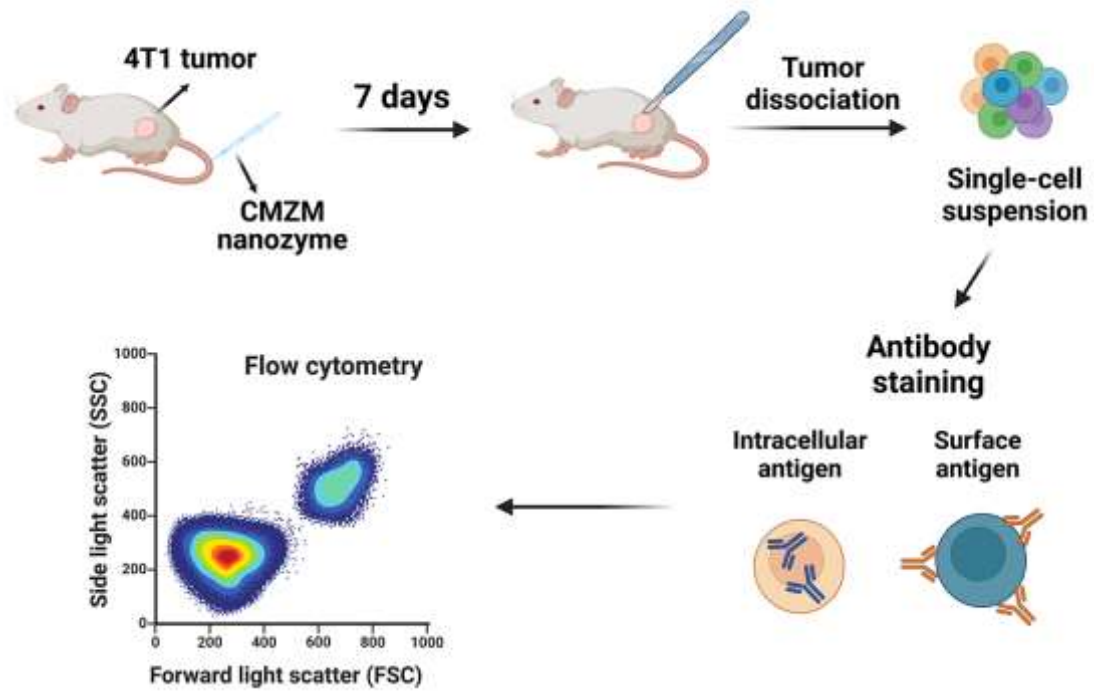


Figure S24. Schedule for determination of *in vivo* immune-activated performances of CMZM by FCM quantitation analysis of macrophages, DC, and T cells in the tumor.

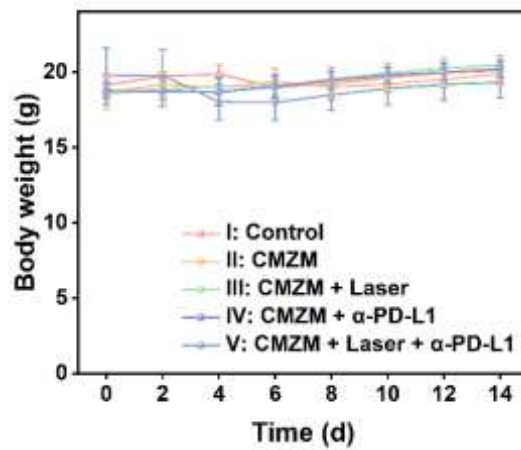


Figure S25. The body weight of 4T1 tumor-bearing mice with different treatments (mean \pm SD, $n = 5$).

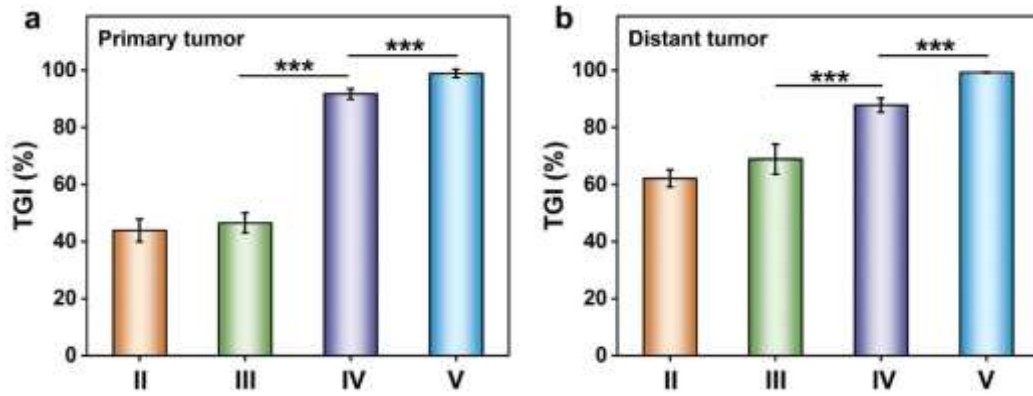


Figure S26. The tumor growth inhibition of 4T1 tumor-bearing mice after various treatments (mean \pm SD, $n = 5$, *** $p < 0.001$).

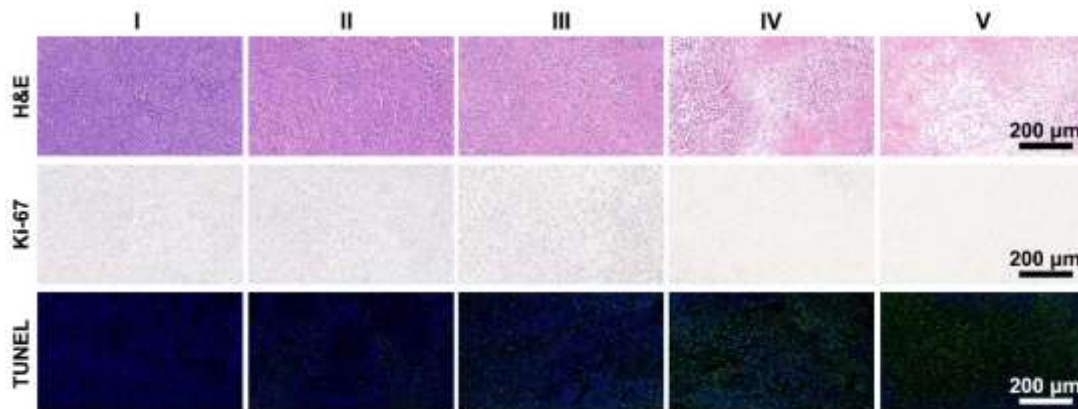


Figure S27. Tumor sections with H&E, TUNEL, and Ki-67 staining after various treatments (I: Control, II: CMZM, III: CMZM + laser, IV: CMZM plus α -PD-L1, and V: CMZM + laser plus α -PD-L1).

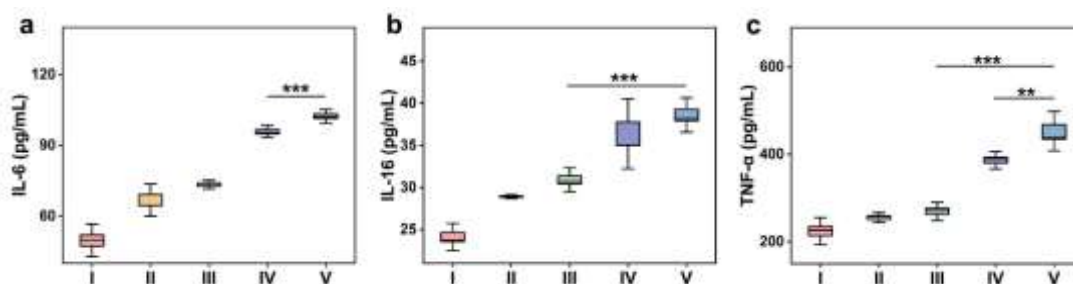


Figure S28. The concentration of IL-6, IL-16, and TNF- α in the supernatant post

various treatments. (I: Control, II: CMZM, III: CMZM + laser, IV: CMZM plus α -PD-L1, and V: CMZM + laser plus α -PD-L1) (mean \pm SD, $n = 3$, $**p < 0.01$, $***p < 0.001$).

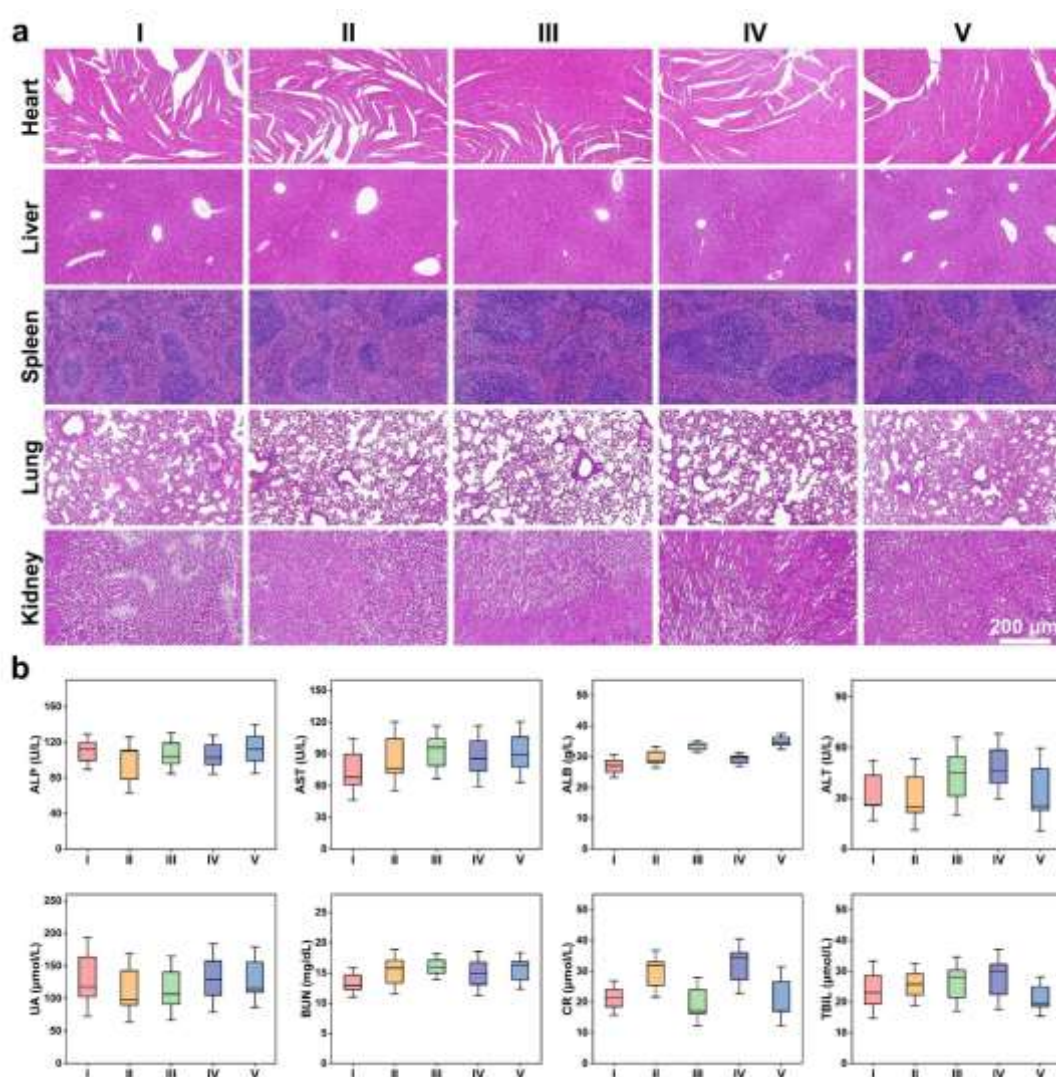


Figure S29. Biosafety evaluation of mice after various treatments (a) H&E staining images of the heart, liver, spleen, lung, and kidney collected from different treatment groups (I: Control, II: CMZM, III: CMZM + laser, IV: CMZM plus α -PD-L1, and V: CMZM + laser plus α -PD-L1). (b) blood indexes of ALP, AST, ALB, ALT, UA, BUN, CR, and TBIL from groups I-V after 14 d treatment (mean \pm SD, $n = 5$).